Available online at www.sciencedirect.com
ScienceDirect
Catalysis Today 126 (2007) 177–183
CATALYSIS TODAY
www.elsevier.com/locate/cattod

Operando Raman study of propane oxidation over alumina-supported V–Mo–W–O catalysts

M.O. Guerrero-Pérez [a], M.C. Herrera [a], I. Malpartida [a], M.A. Larrubia [a], L.J. Alemany [a,*], M.A. Bañares [b]

[a] *Departamento de Ingeniería Química (Unidad Asociada ICP-CSIC), Universidad de Málaga, Campus de Teatinos s/n, E-29071-Málaga, Spain*
[b] *Instituto de Catálisis y Petroleoquímica (CSIC), Marie Curie 2, E-28049-Madrid, Spain*

Available online 11 December 2006

Abstract

The effect of tungsten over Mo–V–O-based catalysts is evaluated. Alumina-supported Mo–V–W–O samples were prepared with different overall metal loading coverages, considering several relative metal atomic ratios; a bulk sample was also synthesized. The catalysts were characterized with BET, XRD, XPS and UV–vis. Mechanistic aspects of the light hydrocarbon oxidation were studied by the *operando* Raman-GC approach. Different surface structures were found and the better propylene yields were achieved when Mo–W and V–W were predominant structures. W incorporation to alumina-supported Mo–V catalysts yields better performance for propane ODH.

Keywords: V–Mo–O; V–Mo–W–O; Nanoscaled oxides; Oxidation; Propane ODH; Structure–activity relationship; *Operando* Raman; XRD; XPS

1. Introduction

Supported metal oxides are widely used in many industrial applications. Mo–V–O oxides are being investigated as catalysts for many oxidation reactions [1], especially for the dehydrogenation (ODH) of light saturated hydrocarbons, as propane [2–6], the ammoxidation to acrylonitrile [7–12] or the selective propane oxidation to acrylic acid [13–15]. The effect of the incorporation of Mo to V-containing catalysts results in a replacement of the polyvanadate structure with less reactive V–O–Mo structure, leading to lower reducibility and oxidative dehydrogenation rates [3,4]. Tungsten is usually added as an additive to the Mo–V–O catalytic system because Mo^{6+} (0.56 Å) and W^{6+} (0.55 Å) ions, as well as V^{4+}, have similar sizes; so, tungsten ions are expected to substitute molybdenum sites [16]. This substitution affects the acid–base, redox and catalytic properties of catalysts. Multimetallic Mo–V–W–O bulk oxides appear promising catalysts for selective oxidation processes [17–22]; this system is claimed as the most selective for the oxidation to acrylic acid from acrolein. At least two different Mo–V–W–O phases have been identified in bulk Mo–V–W–O catalysts [17]. It has been reported that there is an improvement of the catalytic performance in the acrolein oxidation related to the formation of a $(MoVW)_5O_{14}$-type mixed oxide [18,19]. But some additional structures have been identified in these catalysts; especially a $(MoVW)_2O_{5-x}$ structure that appears to be involved in the catalytic cycle [20]. The details of the structure of surface species on these Mo–V–W–O catalysts and the role of the Mo–V–O and Mo–V–W–O mixed phases are not fully understood. The use of *operando* Raman spectroscopy complemented with spectroscopic techniques that is able to obtain Raman spectra of the catalysts under real reaction conditions, would provide the knowledge of the structure of active sites during catalytic operation [23–27].

2. Experimental

The synthesis of the supported catalysts was carried out by one-step incipient wetness impregnation on Al_2O_3 support (Alpha Aesar, 150 m^2/g); using ammonium metanavanadate (NH_4VO_3), ammonium molybdate tetrahydrated ($(NH_4)_2MoO_4 \cdot 4H_2O$) or ammonium metatungstate hydrate ($(NH_4)_6W_{12}O_{39} \cdot xH_2O$) as metals precursors using oxalic acid as complexing

* Corresponding author.
E-mail address: luijo@uma.es (L.J. Alemany).

0920-5861/$ – see front matter © 2006 Elsevier B.V. All rights reserved.
doi:10.1016/j.cattod.2006.10.004

agent. The solution was kept at least for 12 h before impregnation to be sure that it was stabilized. The materials were dried for 12 h at 373 K (100 °C) in air and then calcined at 873 K (600 °C) for 2 h. For the sake of simplicity, all the alumina-supported catalysts are labelled as "xMo$_a$V$_b$W$_c$/Al". Varying the local metal ratio, some catalysts were prepared with an overall loading corresponding to a Mo + V + W coverage of eight atoms for nm^2 of support, value close to the theoretical monolayer of vanadium in alumina [28], labelled with $x = 8$. A catalyst was prepared with a surface metal density of 4, and it was labelled with $x = 4$. For comparative purposes, a bulk sample was synthesized by an oxalic solution containing the precursors that was dried during 2 weeks at ambient temperature; it was calcined similarly to the supported series. Bulk catalyst was labelled as MoVW. 8MoV/Al, 8MoW/Al and 8VW/Al binary samples were prepared with the same methods for comparative purposes.

BET areas were computed from the nitrogen adsorption isotherms recorded on an automatic Micromeritics ASAP-2000 apparatus. X-ray diffraction patterns (XRD) were recorded with a Siemens D-501 diffractometer using Cu Kα radiation (operation value 40 kV and 22.5 mA) registered Bragg's angles between 10° and 70°. UV–vis spectroscopy in diffuse reflectance (UV–vis-RD) was recorded using a Jasco V-570 model spectrometer between the 200–800 nm of wavelength. Spectra were normalized according to Kubelka–Munk function.

The photoelectronic spectra (XPS) were acquired with a Physical Electronic 5700 spectrometer equipped with a hemispherical electron analyser and Mg Kα X-ray exciting source (1253.6 eV, 15 kV, 300 W). The binding energy values (BE) were calculated using the C 1s peak at 284.9 eV. The accuracy of the BE values was ±0.2 eV. A strategy was established for the mathematical deconvolution and in all cases we adjust the signal, after background subtraction, to a mathematical response consistent of a distribution Gaussian–Lorenztian (80–20%, respectively) with a minimum χ^2 error; the contribution of each signal to the global one, expressed as relative percentage is the area under the curve and the maximum of the distribution are associated to the value of the bond energy.

Operando Raman spectra were run with a single-monochromator Renishaw System 1000 equipped with a cooled CCD detector (−73 °C) and holographic super-Notch filter. The samples were excited with a 514 nm Ar line; the spectral resolution was ca. 3 cm^{-1}. The spectra were obtained under reaction conditions in a home-made reaction quartz cell tubing with optical quality walls. Therefore, the fixed-bed catalytic reactor possesses walls that are optically appropriate for Raman spectroscopy. The laser power on the sample was kept very low (below 9 mW) to prevent local heating at the spot of spectral acquisition, which would have made the spectra not representative of the catalyst bed. As a consequence, the signal-to-noise ratio is low and acquisition time was adjusted to compensate (30 scans of 60 s). Representative spectra are shown since several spectra and on-line activity measurements were taken at each temperature. The reactivity was analyzed with an on-line gas chromatograph equipped with a flame-ionization and thermal-conductivity detectors (Varian 3800). The correctness of the analytical determinations was checked for each test by verification that the carbon balance (based on the propane converted) was within the cumulative mean error of the determinations (±10%). Runs were made using 0.2 g of sample with particle size in the 0.25–0.125 mm range. Tests were made using the following feed: 6.2% O_2 and 18.8% propane in helium. The total flow rate was 20 ml/min corresponding to a gas-space velocity (GHSV) of ca. 3000 h^{-1}. Yields and selectivities in products were determined on the basis of the moles of propane feed and products, considering the number of carbon atoms in each molecule (water was not considered). Internal diffusion phenomena were evaluated with a wide range of catalyst particle size. The particle size range of 0.250–0.125 mm showed no internal diffusion. External diffusion phenomena were also studied at different total flows of reactant at constant GHSV, using particle dimensions in the 0.250–0.125 mm range. No external diffusion problems are present for 0.20 g of catalyst using a total flow of 20 mL/min. So, tests were made using 0.20 g of sample with particle dimensions in the 0.250–0.125 mm range [29].

3. Results

Table 1 shows the theoretical composition and BET values of catalysts. It should be noted that similar BET area values are recorded for trimetallic supported catalysts. 8MoVW/Al exhibits the highest BET area value of all the samples with a coverage of one monolayer.

XRD patterns of supported catalysts are shown in Fig. 1; the signal-to-noise ratio is elevated, indicative that samples are not very crystalline. Weak features near 46° and 68° are detected in all patterns and correspond to the amorphous alumina support (JCPDS file 37-1462). A very weak diffraction near 38° is detected in almost all samples and could be associated to different multimetallic segregate oxides containing molybdenum. Also, two weak signals near 23.6° and 34.1°, which appear in the 8MoVW$_2$/Al pattern, can be associated to the most intense peaks of WO_3 oxide (JCPDS file 83-0951). The trimetallic catalyst 8MoVW/Al, with a metal loading close to theoretical monolayer coverage exhibits no diffraction lines.

The electronic profiles (UV–vis-DR) of the samples are shown in Fig. 2. Fig. 2A shows the effect of catalysts composition varying the relative atomic ratio for the supported catalysts. 8Mo$_2$VW/Al, 8MoV$_2$W/Al and 8MoVW$_2$/Al sam-

Table 1
BET surface area and composition of catalysts

	BET area (m^2/g)	Mo/V molar ratio	Mo/W molar ratio	Support
MoVW	5.3	1	1	Bulk
4MoVW/Al	130.1	1	1	Al_2O_3
8MoVW/Al	129.0	1	1	Al_2O_3
8Mo$_2$VW/Al	119.1	2	2	Al_2O_3
8MoV$_2$W/Al	120.2	0.5	1	Al_2O_3
8MoVW$_2$/Al	119.1	1	0.5	Al_2O_3

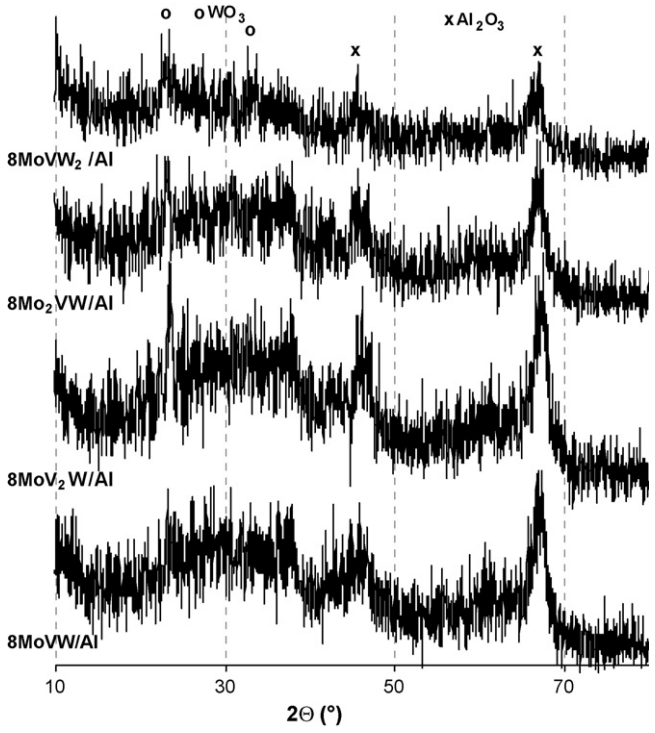

Fig. 1. XRD patters of 8MoVW/Al, $8Mo_2VW/Al$, $8MoV_2W/Al$, $8MoVW_2/Al$ samples.

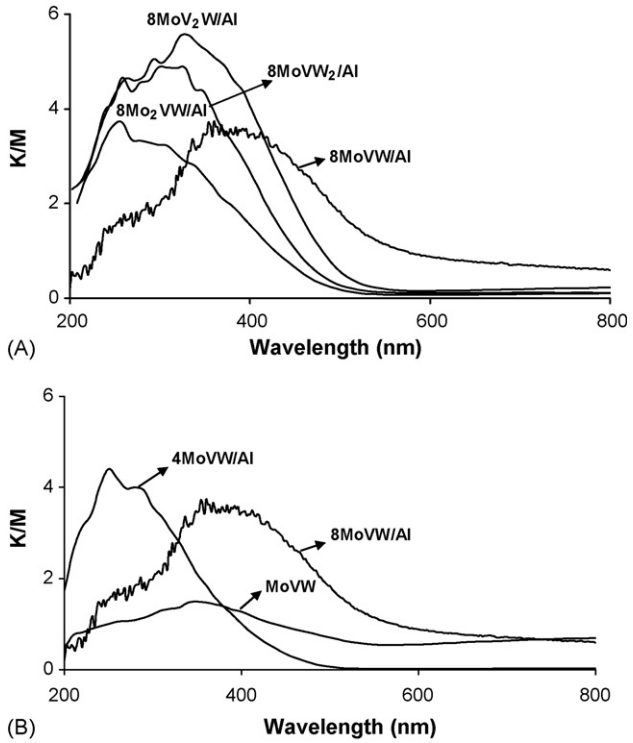

Fig. 2. UV–vis–NIR spectra of 8MoVW/Al, $8Mo_2VW/Al$, $8MoV_2W/Al$, $8MoVW_2/Al$ samples (A) and MoVW, 4MoVW/Al and 8MoVW/Al samples (B).

ples show absorption in the 200–500 nm region, that is associated to charge transfer transitions ($O^{2-} \rightarrow M^{n+}$) [30] from the O 2p valence bands of the supported oxides to the V 3d, Mo 4d and W 5d orbitals, apparently dominated by the charge transfer transition of the majority of metal that has been added. However, with a similar overall metal loading but with Mo/V and Mo/W molar ratio equal to 1, the 8MoVW/Al electronic profile is quite different from the other samples since its maximum shifts to higher wavelengths (390 nm).

Fig. 2B shows the effect of metal coverage. When coverage is near half monolayer (4MoVW/Al sample), the maximum is located near 250 nm and it presents a gap energy higher than 8MoVW/Al. This could be indicative of discrete mixed oligomeric species dispersed on the surface of catalysts with higher coordination, in line with the Raman spectrum (not shown). The Raman spectrum of dehydrated 4MoVW/Al sample presents Raman bands near 1000 and 1020 cm^{-1} sensitive to hydration, characteristic of M=O terminal bonds [27]. On the contrary, the UV–vis spectra of MoVW and 8MoVW/Al samples show absorption at higher wavelengths, indicative of an electronic interaction between the surface oxide species that may occur through oxygen bridging and facilitated by a lower overall coordination [30–32].

Table 2 summarizes the XPS data. For most of the samples, the V 2p signal is contribution of two components. The one at higher binding energy is assigned to V^{5+} species whereas the second at lower binding energy is associated to more reduced species, as V^{4+} [17,32]. Sample 8MoVW/Al presents higher V^{4+} species population than MoVW, 4MoVW/Al, $8Mo_2VW$ and $8MoV_2W/Al$. Only one component is detected for $8MoVW_2$ sample that can be assigned to V^{4+}.

Mo^{6+} and Mo^{5+} surface species led to two unresolved bands close to 235.0 and 232.3 eV; in agreement with the results obtained previously with Mo–V–W samples [17,32]. Mo^{4+} species were detected as a separate contribution close to 234.0 eV. Curve fitting was conducted in order to determine the relative contributions of Mo^{6+}–Mo^{5+} and Mo^{4+} species. Only the Mo^{6+}–Mo^{5+} contribution was detected for MoVW and 4MoVW/Al samples. For the rest of the samples, ($8Mo_2VW/Al$, $8MoV_2W/Al$ and $8MoVW_2/Al$), the relative population of

Table 2
Binding energies (eV)

	V (2p)	Mo (3d)	W (4f)
MoVW	517.3 (82%), 516.2 (18%)	235.9	37.7
4MoVW/Al	516.8	235.3	37.2
8MoVW/Al	517.1 (32%), 515.9 (68%)	235.1 (91%), 233.8 (9%)	37.5
$8Mo_2VW/Al$	516.3 (64%), 515.5 (36%)	235.4 (91%), 234.1 (9%)	37.4
$8MoV_2W/Al$	516.7 (77%), 515.8 (23%)	235.4 (90%), 233.8 (10%)	37.4
$8MoVW_2/Al$	516.1	235.4 (93%), 234.0 (7%)	37.4

Table 3
Propane and oxygen conversions and selectivities to principal reaction products (%) for MoVW, 4MoVW and 8MoVW/Al samples

	Conversion (%)		Selectivity (%)			
	Propane	Oxygen	CH_4	CO	CO_2	Propylene
MoVW	27.5	42.1	0.0	38.7	29.6	31.8
4MoVW/Al	24.1	71.3	1.5	34.4	22.8	41.4
8MoVW/Al	10.5	82.2	0.0	36.2	27.3	36.0

Reaction conditions: 400 °C, total flow 20 ml/min. Reaction feed: 6.2%O2 and 18.8% propane in He. 0.2 g of catalyst.

Mo^{6+}–Mo^{5+} and Mo^{4+} resulted 90/10 (%), respectively. The signal corresponding to W^{6+} species [32] is detected in all samples, indicative that W is in its highest oxidation state.

Table 3 presents activity results obtained for MoVW, 4MoVW/Al and 8MoVW/Al catalysts. 8MoVW/Al presents the lowest propane conversion value and the highest oxygen consumption, whereas 4MoVW/Al sample presents the highest propylene selectivity.

Fig. 3 shows *operando* Raman spectra and catalytic performance during propane ODH of bulk MoVW and alumina-supported 8MoVW/Al samples. The *operando* Raman spectra for 4MoVW/Al catalysts were not obtained due to fluorescence problems. Raman spectra of bulk MoVW catalyst (Fig. 3A) presents intense Raman bands near 962 and 780 cm^{-1} that become more intense during catalytic test. Such bands have been found before [3] and resemble those of α-MoO_3 shifted by ca. 30 cm^{-1}. This would be indicative of a distorted MoO_3 lattice due to some V cations. Raman spectra of supported 8MoVW/Al sample with relative similar composition (Fig. 3B) show two bands near 230 and 1000 cm^{-1} that become more intense when temperature reaction is increased. Such bands have been found before in Mo–V–O supported catalysts [3,4] and usually also appears a less intense band close to 770 cm^{-1} that is hardly visible. Such bands appear for high coverages of Mo and V on the support and have been assigned to a AlVMoO$_7$ structure [4]. These Raman bands resemble those obtained for $K_3PMo_{12}O_{40}$ and α-$K_6P_2W_{18}O_{62}$ samples [33]. $K_3PMo_{12}O_{40}$ presents a Keggin-type structure; it has 12 distorted MoO_6 octahedra surrounding a central phosphate tetrahedron. Every Mo atom presents one terminal short Mo=O with additional Mo–O–Mo bridges and also oxygen atoms triply bridging between one P and two Mo atoms [33]. α-$K_6P_2W_{18}O_{62}$ is a Dawson-type heteropolyanion, where two phosphorus

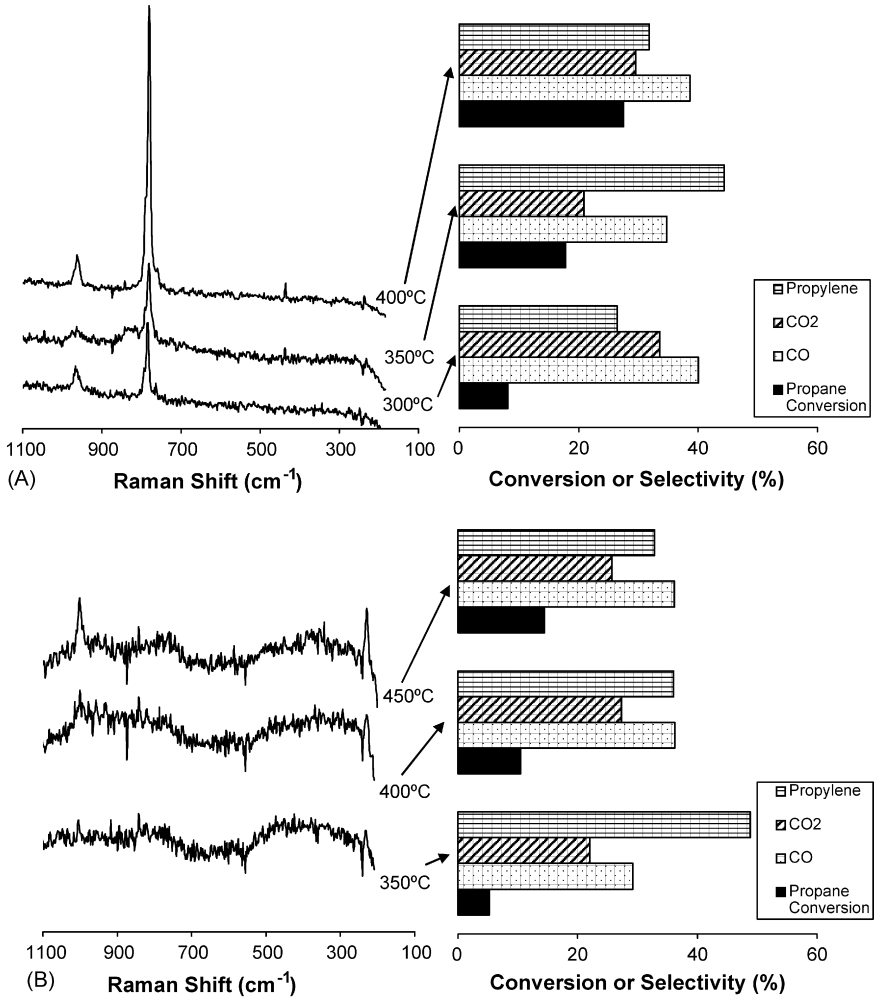

Fig. 3. *Operando* Raman spectra of MoVW (A) and 8MoVW/Al (B) catalysts during propane oxidation and corresponding selectivities to different products and propane conversion values. Reaction condition: 200 mg of catalyst, total flow 20 ml/min, feed composition (% volume): C_3H_8/O_2/He (18.8/6.2/75).

tetrahedral sites are surrounded by 18 distorted tungsten octahedral sites with one terminal W=O bond each [33]. So, both structures are examples of Mo- and W-based heteropolyacids that, in fact, are aggregates of mono-oxo species. A further discussion about the assignment of Raman bands near 230 and 1000 cm^{-1} in this kind of structures can be found in literature [33,34]. Supported 8MoVW/Al sample presents only a metal loading coverage that corresponds to one theoretical monolayer of Mo + V + W on alumina support, that would explain why in our case the Raman bands near 230 and 1000 cm^{-1} are less intense that those found in literature with bulk samples. So, 8MoVW/Al could present disperse polymeric mono-oxo structure, similar to the structure of a heteropolyacid, in line with the UV–vis results, which underline an electronic interaction between surface oxide species. It should be noted that 8MoVW/Al sample is the only one in which the majority of vanadium species remain reduced as V(IV) according to the XPS data (Table 2).

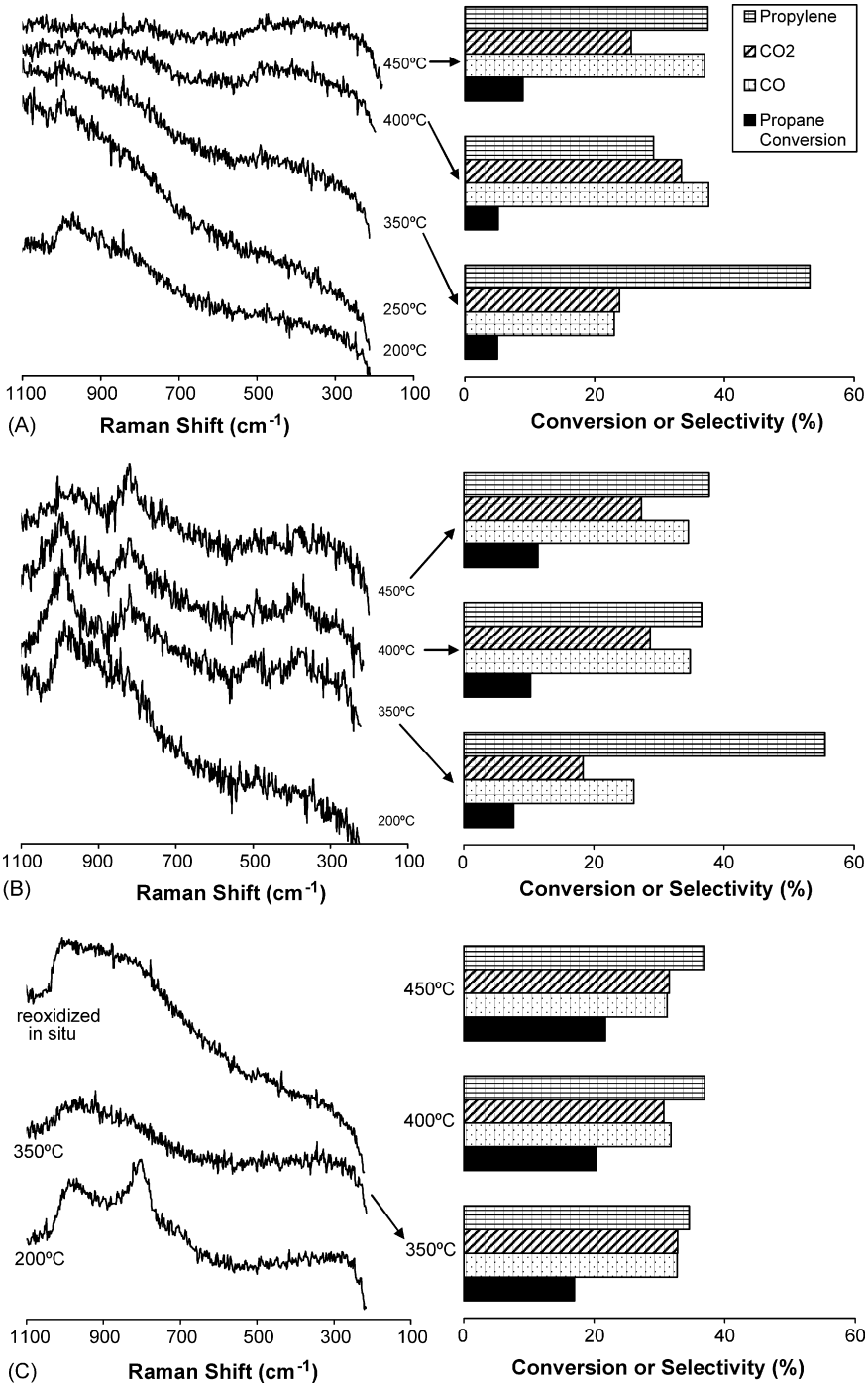

Fig. 4. *Operando* Raman spectra of $8MoV_2W/Al$ (A), $8Mo_2VW/Al$ (B) and $8MoVW_2/Al$ (C) catalysts during propane oxidation and corresponding selectivities to different products and propane conversion values. Reaction conditions: 200 mg of catalyst, total flow 20 ml/min, feed composition (% volume): $C_3H_8/O_2/He$ (18.8/6.2/75).

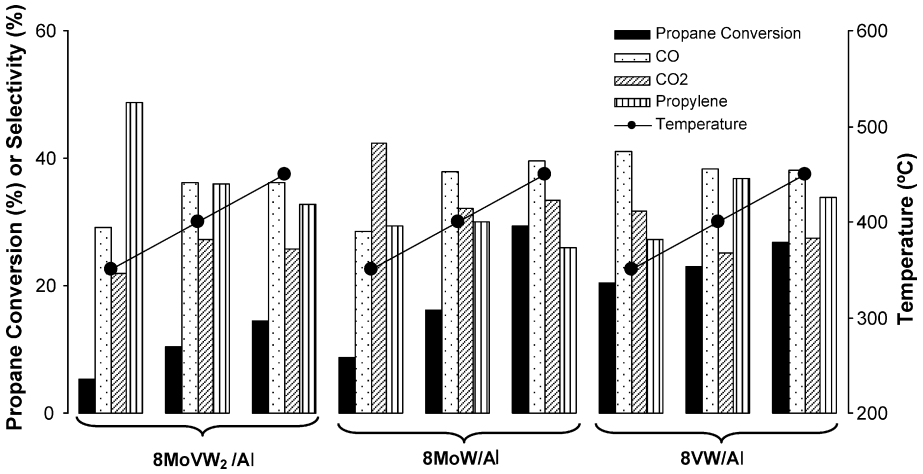

Fig. 5. Propane conversion and selectivities to principal products obtained at three temperatures for samples $8MoVW_2$/Al, 8MoW/Al and 8VW/Al. Reaction conditions: 200 mg of catalyst, total flow 20 ml/min, feed composition (% volume): C_3H_8/O_2/He (18.8/6.2/75).

Fig. 4 shows *operando* Raman spectra and their on-line simultaneous catalytic results for $8Mo_2VW$/Al, $8MoV_2W$/Al and $8MoVW_2$/Al. The Raman spectrum at 200 °C of $8MoV_2W$/Al (Fig. 4A) shows a broad feature between 950 and 1030 cm^{-1}. The Mo=O stretching mode at 990 cm^{-1} of surface mono-oxo molybdenum oxide species [27], and the V=O [27] and W=O [35] stretching modes near 1030 and 1000 cm^{-1}, respectively, should appear in that region. Apparently, these surface species must be interacting intensely so that no clear Raman band becomes apparent. These bands are not visible when the reaction temperature increases, mainly due to the fluorescence background. The Raman spectrum of $8Mo_2VW$/Al (Fig. 4B) at 200 °C shows a similar broad feature between 950 and 1030 cm^{-1}, which disappears with reaction temperature. When reaction temperature increases, a broad Raman band becomes evident near 830 cm^{-1}. Similar spectra were obtained with Mo/Al_2O_3 catalysts during methanol oxidation in absence of oxygen by Payen and co-workers [36]. They attributed the band near 830 cm^{-1} to reduced sites [36]; in accordance with other authors that associate Raman bands in the 800–950 cm^{-1} region with reduced molybdenum oxide species [17–18,37].

The Raman spectrum of $8MoVW_2$/Al (Fig. 4C) at 200 °C shows a very distorted and broad Raman band near 810 cm^{-1} that correspond to the most intense band of WO_3 microcrystalline phase [35], in line with the XRD results. As in the case of $8Mo_2VW$/Al and $8MoV_2W$/Al samples, a broad feature between 950 and 1030 cm^{-1} is apparent. WO_3 microcrystalline surface aggregates tend to disperse during catalytic reaction and the Raman signal of WO_3 is no longer visible. After catalytic runs, the sample was reoxidized *in situ*, generating a broad feature between 950 and 1030 cm^{-1}. This catalyst presents the best catalytic behaviour in this series; the propylene selectivity is almost the same than for $8Mo_2VW$/Al and $8MoV_2W$/Al but it reaches higher propane conversion. Fig. 5 presents the catalytic activity data obtained for samples with the same tungsten loading: 8MoW/Al, 8VW/Al and $8MoVW_2$/Al. Supported binary samples 8MoW/Al and 8VW/Al possess crystalline WO_3 phase [32]. Fig. 5 shows that 8MoW and 8VW are both more active than the ternary sample $8MoVW_2$/Al, but the ternary catalyst is most selective for propylene at all the temperatures studied. The *operando* Raman spectra of the binary 8MoW/Al and 8VW/Al samples did not change during catalytic operation and they are not showed here for brevity.

4. Discussion

The loading coverage drastically affects both structure and performance (Fig. 3) of catalysts. Bulk MoVW and supported 8MoVW/Al samples present well-defined structures. The bulk sample presents a distorted α-MoO_3 lattice due to the partial insertion of some V cations whereas the supported sample probably presents a heteropolyacid-type sites coordination. 4MoVW/Al sample presents dispersed oxide surface structures with lower polymerization degree among metallic sites than at higher coverages. The 8MoVW/Al sample exhibits the lowest activity in this series (Table 3). The *operando* experiments show that the heteropolyacid structure develops during reaction and remains stable during catalytic operation (Fig. 3B). It has been described that well-defined Mo-based polyacids are not the active species in an operating partial oxidation catalysts [38]. 4MoVW/Al sample presents the highest propylene selectivity of this series (Table 3). This is consistent with previous results reporting higher propylene selectivities at low metal coverages on alumina support [3].

The catalysts composition affects both structure and reactivity (Fig. 4) of catalysts. The Raman profile of $8Mo_2VW$/Al and $8MoV_2W$/Al are quite similar at low temperatures, but the formation of reduced molybdenum species is detected during propane ODH for $8Mo_2VW$/Al catalysts (Fig. 4B); however, those catalyst present a similar catalytic behaviour, with very low propane conversion. Vanadium [39] or molybdenum [40] catalysts are mainly selective to COx. Mestl et al. found that the selectivity to partial oxidation products is improved with Mo–W and Mo–V–W catalytic systems. So, in order to achieve better propylene selectivity, a higher amount of W should be incorporated in the catalysts formulation, as expected, catalysts with a higher

tungsten loading lead to higher propylene selectivity (Fig. 4C). Fig. 5 shows that the binary samples 8MoW/Al and 8VW/Al are more active than the ternary $8MoVW_2$/Al counterpart, indicative that Mo–V–O bonds are less reactive than Mo–W and V–W ones. The structure of the binary samples is discussed in a previous paper [32] and it was found that both posses a tungsten oxide structure with a Raman spectrum similar to that obtained for $8MoVW_2$/Al sample.

A difference of the results found in literature about Mo-based structures that showed that Mo-based polyacids are not the active species during partial oxidation reactions [38]; the results about polytungstates structures show that they are active and selective catalysts in oxidation reactions [41,42]. This fact could explain why in present paper tungsten-based structures present better catalytic results than the Mo-based structures.

The V/Al system yields total oxidation and is not efficient for partial oxidation. When Mo is incorporated, the V–O–V structures in polyvanadates are replaced by less reactive V–O–Mo, leading to lower oxidative ODH rates, as have been described previously by Iglesia and co-workers [4]. The results presented here prove tungsten as a good additive for V-based catalysts. It has been demonstrated that different Mo-based structures (the α-MoO_3 lattice distorted as well as the heteropolyacid-type structure) do not lead to better catalytic selective oxidation performance, on the contrary, Mo–W–O and V–W–O-based structures exhibit higher propylene yields.

5. Conclusions

Tungsten addition to Mo–V–O-based catalysts affords better performance during propane ODH. The structure of such catalysts depends of both Mo + V + W total coverage and Mo/V and Mo/W molar ratio. Different Mo-based structures were found, but better propylene yields are reached when Mo–W–O and V–W–O predominate. Therefore, tungsten should be added as a majoritary component in the catalysts formulation in order to achieve selective catalysts towards propylene.

Acknowledgements

This research was funded by Ministry of Education and Science (Spain) projects ENE2004-06176, CTQ2004-06045 and CTQ2005-02802/PPQ. MOGP acknowledges Ministry of Education and Science (Spain) for a ‘‘Juan de la Cierva’’ postdoctoral position. The authors thank Dr. C. Resini (Università di Genova, Italy), for his help with UV–vis spectroscopy.

References

[1] A. Bielanski, M. Najbar, Appl. Catal. A 157 (1997) 223.
[2] J.D. Pless, B.B. Bardin, H.S. Kim, D. Ko, M.T. Smith, R.R. Hammond, P.C. Stair, K.R. Poeppelmeier, J. Catal. 223 (2004) 419.
[3] M.A. Bañares, S.J. Khatib, Catal. Today 96 (2004) 251.
[4] S. Yang, E. Iglesia, A.T. Bell, J. Phys. Chem. B 109 (2005) 8987.
[5] Z. Zhao, X. Gao, I.E. Wachs, J. Phys. Chem. B 107 (2003) 6333.
[6] P. Botella, E. García-González, A. Dejoz, J.M. López Nieto, M.I. Vázquez, J. González-Calbet, J. Catal. 225 (2004) 428.
[7] J.M. Millet, H. Roussel, A. Pigamo, J.L. Dubois, J.C. Jumas, App. Catal. 232 (2002) 77.
[8] M. Vaarkamp, T. Ushikubo, App. Catal. A: Gen. 174 (1998) 99.
[9] H. Tsuji, Y. Koyasu, J. Am. Chem. Soc. 124 (2002) 5608.
[10] M.O. Guerrero-Pérez, J.N. Al-Saeedi, V.V. Guliants, M.A. Bañares, App. Catal. A 260 (2004) 93.
[11] M. Baca, J.-M.M. Mollet, App. Catal. A 279 (2005) 67.
[12] H. Watanabe, Y. Koyasu, App. Catal. A 194–195 (2000) 479.
[13] V.V. Guliants, R. Bhandari, J.N. Al-Saeedi, V.K. Vasudevan, R. Soman, O. Guerrero-Pérez, M.A. Bañares, Appl. Catal. A 274 (2004) 123.
[14] J.N. Al-Saeedi, V.V. Guliants, M.O. Guerrero-Pérez, M.A. Bañares, J. Catal. 215 (2003) 108.
[15] W. Ueda, D. Vitry, T. Katou, Catal. Today 96 (2004) 235.
[16] J.D. Pless, H.-S. Kim, J.P. Smit, X. Wang, P.C. Stair, K.R. Poeppelmeier, Inorg. Chem. 45 (2006) 514.
[17] G. Mestl, Ch. Linsmeier, R. Gottschall, M. Dieterle, J. Find, D. Herein, J. Jäger, Y. Uchida, R. Schlögl, J. Mol. Catal. A 162 (2000) 463.
[18] M. Dieterle, G. Mestl, J. Jäger, Y. Uchida, H. Hibst, R. Schlögl, J. Mol. Catal. A 174 (2001) 169.
[19] O. Ovsitser, Y. Uchida, G. Mestl, G. Weinberg, A. Blume, J. Jäger, M. Dieterle, H. Hibst, R. Schlögl, J. Mol. Catal. A 185 (2002) 291.
[20] T. Uchida, G. Mestl, O. Ovsitser, J. Jäger, A. Blume, R. Schlögl, J. Mol. Catal. A: Chem. 187 (2002) 247.
[21] L.J. Alemany, M.C. Jimenez, E. Pardo, J. Machek, S. Svachula, React. Kinet. Catal. Lett. 51 (1993) 383.
[22] J. Svachula, L.J. Alemany, M.A. Larrubia, J. Tichy, React. Kinet. Catal. Lett. 49 (1993) 145.
[23] B.M. Weckhuysen, Chem. Commun. 97 (2002) 97.
[24] M.O. Guerrero-Pérez, M.A. Bañares, Chem. Commun. 12 (2002) 01292.
[25] M.O. Guerrero-Pérez, M.A. Bañares, Catal. Today 113 (2006) 48.
[26] M.A. Bañares, M.O. Guerrero-Pérez, J.L.G. Fierro, G.G. Cortez, J. Mater. Chem. 12 (2002) 3337.
[27] M.A. Bañares, I.E. Wachs, J. Raman Spectrosc. 33 (2002) 359.
[28] I.E. Wachs, L.E. Briand, J.-M. Jehng, L. Burcham, X. Gao, Catal. Today 57 (2000) 323.
[29] M.O. Guerrero-Pérez, M.A. Peña, J.L.G. Fierro, M.A. Bañares, Ind. Eng. Chem. Res. 45 (2006) 4537.
[30] M.A. Larrubia, G. Busca, Mat. Chem. Phys. 72 (2001) 337.
[31] M.A. Bañares, M.V. Martínez-Huerta, X. Gao, J.L.G. Fierro, I.E. Wachs, Catal. Today 61 (2000) 295.
[32] M.O. Guerrero-Pérez, M.C. Herrera, I. Malpartida, M.A. Larrubia, L.J. Alemany, Catal. Today 118 (2006) 360–365.
[33] G. Busca, J. Raman Spectrosc. 33 (2002) 348.
[34] C. Rocchiccioli-Deltcheff, A. Aouissi, S. Launay, M. Fournier, J. Mol. Catal. A 114 (1996) 331.
[35] D.S. Kim, M. Ostromecki, I.E. Wachs, J. Mol. Catal. A 106 (1996) 93.
[36] M. Brandhorst, S. Cristol, M. Capron, C. Dujardin, H. Vezin, G. Le bourdon, E. Payen, Catal. Today 113 (2006) 34.
[37] G. Mestl, T.K.K. Srinivasan, Catal. Rev. Sci. Eng. 40 (1998) 451.
[38] G. Mestl, T. Ilkenhans, D. Spielbauer, M. Dieterle, O. Timpe, J. Kröhnert, F. Jentoft, H. Knözinger, R. Schlögl, Appl. Catal. A 210 (2001) 13.
[39] M.O. Guerrero-Pérez, J.L.G. Fierro, M.A. Bañares, Catal. Today 118 (2006) 366–372.
[40] G. Mestl, J. Raman Spectrosc. 33 (2002) 333.
[41] S. Casuscelli, E. Herrero, M. Crivello, C. Pérez, M.G. Egusquiza, C.I. Cabello, I.L. Botto, Catal. Today 107–108 (2005) 230.
[42] R. Neumann, M. Gara, J. Am. Chem. Soc. 116 (1994) 5509.